Roton-type mode softening in a quantum gas with cavity-mediated long-range interactions

R. Mottl, F. Brennecke, K. Baumann, R. Landig, T. Donner, and T. Esslinger*

Institute for Quantum Electronics, ETH Zürich, 8093 Zürich, Switzerland

Long-range interactions in quantum gases are predicted to give rise to an excitation spectrum of roton character, similar to that observed in superfluid helium. We investigate the excitation spectrum of a Bose-Einstein condensate with cavity-mediated long-range interactions, which couple all particles to each other. Increasing the strength of the interaction leads to a softening of an excitation mode at a finite momentum, preceding a superfluid to supersolid phase transition. We study the mode softening spectroscopically across the phase transition using a variant of Bragg spectroscopy. The measured spectrum is in very good agreement with ab initio calculations and, at the phase transition, a diverging susceptibility is observed. The work paves the way towards quantum simulation of long-range interacting many-body systems.

PACS numbers: 37.30.+i, 42.50.-p, 05.30.Rt

Experiments with ultracold gases have succeeded in realizing a variety of quantum many-body phases by exploiting the tunability of short-range atom-atom interactions [1]. Creating quantum gases with long-range interactions [2–5] is motivated by the prospect of observing previously unexplored phenomena and phases [6]. In particular, long-range interactions in a Bose-Einstein condensate (BEC) have been predicted [7–10] to give rise to an excitation spectrum similar to the roton spectrum observed in superfluid helium [11]. A roton spectrum emerges from density-density correlations which can be induced by short-range van-der-Waals interactions as in liquid helium or by momentum-dependent long-range interactions in dilute quantum gases [7]. Such a mode softening at finite momentum has been proposed as a possible route to a supersolid phase [12].

Important steps towards realizing quantum gases with long-range interactions have been achieved by cooling atomic species with large magnetic dipole moment to quantum degeneracy [2, 5] and by the efforts to prepare ultracold polar molecules in their ground state [3, 4]. Effects of long-range interactions in quantum gases have been observed in the anisotropic expansion, in collective as well as Bloch oscillations, and in the stability of interacting dipolar BEC [13–16]. However, a roton-type mode softening requires very strong long-range interactions and is challenging to observe in quantum gases.

A different approach to long-range interactions in cold gases makes use of the radiative coupling between electric dipoles induced by off-resonant laser light, which has been shown theoretically to cause a roton-like minimum in the energy spectrum of a BEC [8, 10]. A large enhancement of such radiative coupling is achieved by placing the dipoles into an optical resonator, which leads to strong global atom-atom interactions [17, 18, 20, 33].

We create long-range interactions in a BEC by placing it into an optical high-finesse cavity and irradiating the atoms with a transverse pump laser, which is far detuned from the atomic transition frequency [21, 32, 36]
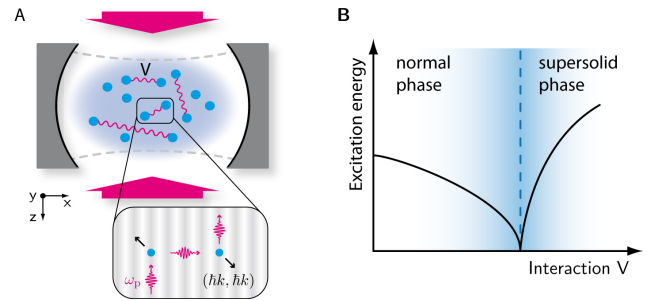

FIG. 1. Experimental scheme and mode softening. (**A**) A ^{87}Rb BEC inside a Fabry-Perot resonator is transversally illuminated by a far red-detuned standing-wave laser field. In a quantized picture, atoms off-resonantly scatter photons from the pump field into a close-detuned TEM$_{00}$ cavity mode and back at rate $NV/\hbar$ (see text), creating and annihilating pairs of atoms in the superposition of momenta $(p_x, p_z) = (\pm\hbar k, \pm\hbar k)$ (see close-up displaying one of four possible processes). This results in global interactions between all N atoms. The interaction strength V is controlled via the power of the transverse laser field. (**B**) The cavity-mediated atom-atom interaction causes a softening of a collective excitation mode at momenta $(\pm\hbar k, \pm\hbar k)$, and a diverging susceptibility (blue shade) at a critical interaction strength (dashed line).

(Fig. 1A). The induced electric dipoles of the atoms oscillate at the pump laser frequency and collectively couple to a single cavity mode, which is detuned from the pump frequency by a few cavity linewidths. In turn, the induced cavity field leads to an ac Stark shift in the atoms. The resulting atom-atom interaction extends over the entire atomic cloud and is tunable in strength. For a critical strength of the long-range interactions, the BEC undergoes a quantum phase transition to a supersolid phase with checkerboard density order [36], as observed in [32]. At the phase transition a discrete spatial symmetry provided by the cavity mode structure is broken, thus establishing nontrivial diagonal long-range order. We have

developed a method to measure the excitation spectrum across this phase transition. The method combines Bragg spectroscopy [24] and cavity-enhanced Bragg scattering, and we use it to observe a notable change in the dispersion relation while crossing the phase transition. This is complemented by a diverging susceptibility, in agreement with the second-order nature of the phase transition (Fig. 1B).

The cavity-mediated long-range interaction is described by the Hamiltonian
$\hat{H}_{aa} = \int \hat{\Psi}^{\dagger}(\mathbf{r})\hat{\Psi}^{\dagger}(\mathbf{r}')\mathcal{V}(\mathbf{r},\mathbf{r}')\hat{\Psi}(\mathbf{r}')\hat{\Psi}(\mathbf{r})d^3\mathbf{r}d^3\mathbf{r}'$ with atomic field operator $\hat{\Psi}(\mathbf{r})$. This Hamiltonian is obtained from the dispersive atom-light interaction Hamiltonian by adiabatically eliminating the fast cavity field dynamics [25, 33]. The interaction potential has the form

$$\mathcal{V}(\mathbf{r},\mathbf{r}') = V\cos(kx)\cos(kz)\cos(kx')\cos(kz') \quad (1)$$

and describes the ac Stark shift experienced by an atom at position $\mathbf{r}$ as a result of the cavity field induced by a second atom at position $\mathbf{r}'$. As a consequence of the interference between the mediating cavity field and the transverse pump field, the spatial dependence of the interaction is determined by the corresponding mode functions $\cos(kx)$ and $\cos(kz)$, where $k = 2\pi/\lambda$ denotes the optical wavevector (Fig. 1A). The interaction strength $V = \hbar\eta^2/\tilde{\Delta}_c$ depends on the two-photon Rabi frequency η which can be tuned experimentally via the transverse pump power P [25]. The sign of V is determined by the detuning $\tilde{\Delta}_c = \omega_p - \tilde{\omega}_c$ between the transverse pump laser frequency ω_p and the dispersively shifted cavity resonance $\tilde{\omega}_c$. In the experiment $|\tilde{\Delta}_c|$ is large compared to the cavity linewidth 2κ.

For negative V, the cavity-mediated interaction induces density correlations in the atomic cloud with spatial periodicity of λ along the pump and cavity direction. In momentum space, this corresponds to the creation and annihilation of pairs of correlated atoms in the momentum mode $|e\rangle$, which is the symmetric superposition of the four momentum states $|p_x, p_z\rangle = |\pm\hbar k, \pm\hbar k\rangle$. For a macroscopically populated zero-momentum mode containing N atoms, this is described by the Hamiltonian [25]

$$\hat{H} = 2E_r\hat{c}^{\dagger}\hat{c} + \frac{NV}{4}(\hat{c}^{\dagger} + \hat{c})^2, \quad (2)$$

where $\hat{c}^{\dagger}$ creates particles in mode $|e\rangle$. The first term in Eq. 2 corresponds to the kinetic energy of atoms in mode $|e\rangle$, with the recoil energy $E_r = \frac{\hbar^2 k^2}{2m}$ and the atomic mass m.

The elementary excitations of the Hamiltonian $\hat{H}$ are of collective nature and their eigenenergy E_s softens for increasing interaction strength V (Fig. 1B). The excitation energy E_s vanishes at a critical interaction strength V_{cr}, where interaction and kinetic energy are balanced, i.e. $N|V_{cr}| = 2E_r$. This marks the transition point between a normal and a supersolid phase. In the supersolid
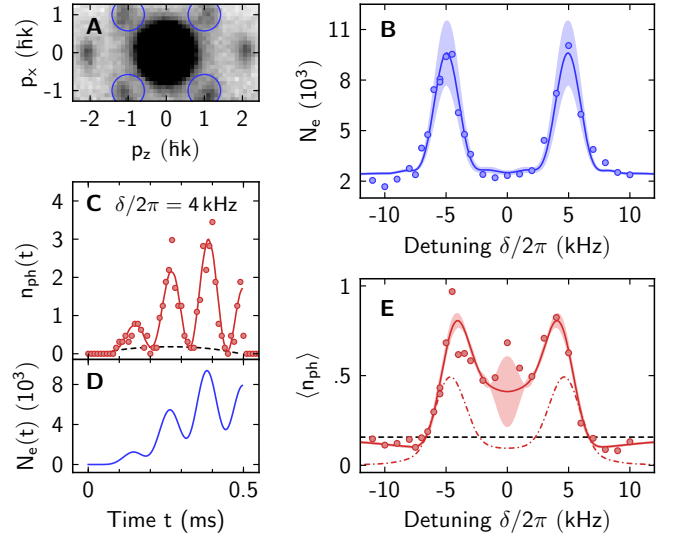

FIG. 2. Probing the excitation spectrum in the normal phase ($P = 0.65P_{cr}$). (**A**) Absorption image of the atomic cloud after probing the cavity for 0.5 ms and subsequent ballistic expansion over 7 ms. (**B**) Excited atomic population N_e with momenta $(\pm\hbar k, \pm\hbar k)$, deduced from the regions enclosed by blue circles in A, as a function of the probe-pump detuning δ (circles). The solid line shows a fit, based on the theoretical model (see text). The background in N_e originates from a residual thermal component extending into the detection region. (**C**) Recorded (circles) and fitted (solid line) mean intracavity photon number n_{ph} during probing. The dashed line indicates the intracavity photon number of the probe pulse, obtained in the absence of atoms. (**D**) Temporal evolution of $N_e(t)$ inferred theoretically from the fit shown in C. (**E**) Mean intracavity photon number $\langle n_{ph}\rangle$, averaged over the probe interval, as a function of δ (circles). The fit (solid line) takes into account the calibrated photon number of the probe pulse (dashed line). From the recorded photon signal we deduce the photon number originating from Bragg scattering off the created excitations (dashed-dotted line). The shading in B and E indicates the fluctuations caused by variations of the relative phase φ between different experimental runs. The detuning of the pump beam from the empty cavity resonance was $\Delta_c = -2\pi \times 18$ MHz and the total atom number $N = 1.6(2) \times 10^5$. The damping constant γ was set to 0.6 kHz (see text).

phase, a macroscopic occupation of the mode $|e\rangle$ gives rise to a checkerboard pattern in the atomic density distribution, which is accompanied by the build-up of a coherent cavity field amplitude α_0. The energy of collective excitations rises again with increasing interaction strength and approaches the single-particle excitation energy of the induced optical checkerboard potential.

To measure the excitation spectrum of the system at momenta $(\pm\hbar k, \pm\hbar k)$, we perform a variant of Bragg spectroscopy [24, 26]. After preparing the system at a given interaction strength, the cavity field is excited with a weak probe pulse along the x-axis (Fig. 1A). Interference between the cavity probe field and the transverse

pump field results in an amplitude-modulated lattice potential $\eta\sqrt{n_{\mathrm{pr}}}\cos(\delta t + \varphi)\cos(kx)\cos(kz)$, with probe-pump detuning $\delta = \omega_{\mathrm{pr}} - \omega_{\mathrm{p}}$, relative phase φ and mean intracavity photon number n_{pr} of the probe field. In momentum space, this corresponds to the perturbation $\hat{H}_{\mathrm{pr}} = \eta\sqrt{n_{\mathrm{pr}}N}\cos(\delta t + \varphi)(\hat{c}^\dagger + \hat{c})$. After probing, all laser fields are switched off. This projects the created collective excitations onto the free-space momentum states $|\pm\hbar k, \pm\hbar k\rangle$, which are detected via absorption imaging subsequent to ballistic expansion (Fig. 2A). A typical resonance curve of the excited momentum state population $N_{\mathrm{e}} = \langle\hat{c}^\dagger\hat{c}\rangle$ as a function of δ is shown in Fig. 2B. Clear resonances are revealed both for positive and negative probe-pump detuning, corresponding to stimulated scattering of probe photons into the pump field and vice versa. The corresponding resonance frequency $E_{\mathrm{s}}/\hbar$ is obtained from a fit (solid line) based on the model description Eq. 2 [25].

The measured excitation spectrum as a function of pump power P is displayed in Fig. 3. When increasing the interaction strength in the normal phase towards the critical point, the excitation energy E_{s} exhibits a distinct softening. In contrast, for positive V, the excitation gap is observed to increase with interaction strength in accordance with the absence of a phase transition. The increasing gap reflects the tendency of the cavity-mediated interactions to suppress density fluctuations with λ-periodicity.

We monitor the cavity output light on a single-photon counting module. This gives us real-time access to the formation of collective excitations during probing. Because of matter-wave interference between the ground-state component of the condensate and the created excitations, a spatial density modulation evolves in time. Transverse pump light is Bragg scattered by this density modulation into the cavity mode. The output from the cavity therefore follows the oscillatory evolution of this density modulation (Fig. 2C). The total intracavity photon number, averaged over the probe interval, again exhibits a double resonance (Fig. 2E), whose characteristic shape has its origin in interference between the probe field (dashed) and the Bragg scattered pump field (dashed-dotted). This provides a second method to determine the resonance frequency $E_{\mathrm{s}}/\hbar$, as shown in Fig. 3.

We model the dynamics of the system during probing by evolving the Hamiltonian $\hat{H} + \hat{H}_{\mathrm{pr}}$ in time, taking into account the recorded shape of the probe pulse, see Fig. 2C. Quantitative agreement with the data is obtained by including a phenomenological damping rate γ in the time evolution of $\hat{c}$ [25]. The corresponding time evolution of the momentum population $N_{\mathrm{e}}(t)$ is shown in Fig. 2D. Depending on the relative phase φ, which is not controlled in the experiment, the phase of the excited density oscillation varies between different experimental runs. This leads to an intrinsic fluctuation of the quantities N_{e} and $\langle n_{\mathrm{ph}}\rangle$, as indicated by the shaded areas in
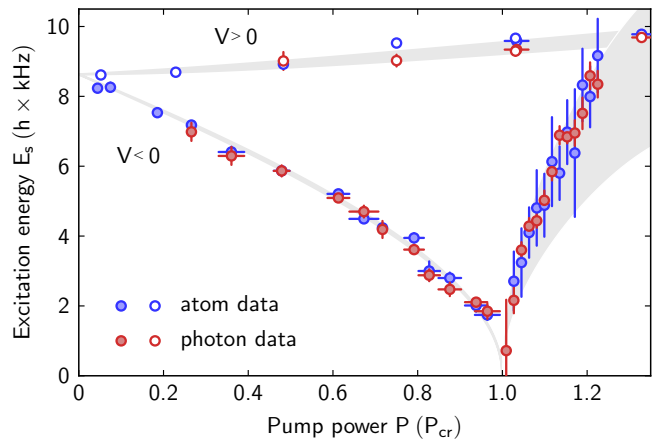

FIG. 3. Excitation spectrum. Measured resonance frequencies E_{s}/h, obtained from atomic (N_{e}) and photonic ($\langle n_{\mathrm{ph}}\rangle$) signals, are shown in blue and red, respectively, for positive (open circles) and negative (filled circles) interaction strength V. Gray shading shows the theoretical prediction including experimental uncertainties [25]. The experimental parameters are $N = 1.7(2) \times 10^5$, $\Delta_{\mathrm{c}} = -2\pi \times (19.8, 23.2)\,\mathrm{MHz}$ for $V < 0$ (normal and supersolid phase) and $\Delta_{\mathrm{c}} = +2\pi \times 15.1\,\mathrm{MHz}$ for $V > 0$. For $V > 0$, the pump power is scaled in terms of the critical pump power observed for $\Delta_{\mathrm{c}} = -2\pi \times 19.7\,\mathrm{MHz}$.

Fig. 2B and E.

In the supersolid phase, the perturbation creates excitations on top of the macroscopic steady-state population in momentum mode $|\mathrm{e}\rangle$ [32]. Because of matter-wave interference, the detected population N_{e} is strongly affected by fluctuations of the relative phase φ. Yet, the variance of N_{e} around the steady-state value, deduced from several experimental runs, shows clear resonances. Alternatively, we use the oscillation amplitude of the intracavity photon number around the steady-state value $|\alpha_0|^2$ to extract the excitation energy E_{s} [25]. As shown in Fig. 3, the excitation energies deduced from these two signals rise again with pump power P and provide a consistent picture.

The observed excitation spectrum (Fig. 3) is in qualitative agreement with a soft mode energy $E_{\mathrm{s}} = 2E_{\mathrm{r}}\sqrt{1 + V/|V_{\mathrm{cr}}|}$ which follows from Eq. 2. Quantitative agreement is obtained by further taking into account the lattice potential of the transverse pump beam as well as contact interactions between colliding atoms [25]. Accordingly, the single-particle mode $|\mathrm{e}\rangle$ in Eq. 2 is replaced by a Bogoliubov mode $|1\rangle$ and the interaction energy gets renormalized by the matrix element of $\mathcal{V}(\mathbf{r}, \mathbf{r}')$ between the condensate mode and the excited state $|1\rangle$. In the normal phase, the state $|1\rangle$ lies in the lowest energy band of the transverse lattice potential with quasi-momentum $(\pm\hbar k, \pm\hbar k)$ and bare energy E_1. For $P = 0$ the excitation energy E_{s} reaches the Bogoliubov energy $E_1 = h \times 8.7\,\mathrm{kHz}$, which is shifted by the mean-field energy with respect to the kinetic energy $2E_{\mathrm{r}} = h \times 7.5\,\mathrm{kHz}$.
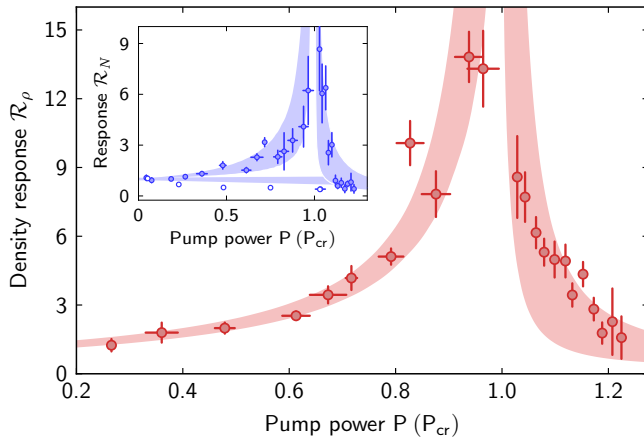
FIG. 4. Response to density perturbations. Shown is the density response in the normal and supersolid phase, normalized to the non-interacting case ($P = 0$). The shaded areas show the theoretical prediction including experimental uncertainties and fluctuations caused by the uncontrolled relative phase φ. The atomic damping constant $\gamma = 2\pi \times 0.5(1)\,\mathrm{kHz}$ was obtained from the fit to the data in the normal phase. The inset shows the response of the excited momentum state population N_e for negative (filled circles) and positive (open circles) interaction strength V. The experimental parameters were the same as in Fig. 3.

In the supersolid phase, the Bogoliubov mode $|1\rangle$, which is dominantly affected by the long-range interactions, lies in a higher energy band at zero quasi-momentum of the emerging checkerboard lattice potential. As a result of competition between the increasing band energy and the renormalized interaction energy, the excitation energy E_s rises again.

Another signature for a softened dispersion relation at finite momentum is provided by the susceptibility to external density perturbations. In terms of the static structure factor $S(k)$, which measures the density-density response, this is expressed by Feynman's relation $S(k) = (\hbar k^2/2m)/\omega(k)$, where $\omega(k)$ denotes the dispersion of a homogeneous system [27]. To determine the density response in our system, we quantify the amount of pump light which is Bragg scattered into the cavity. This allows us to measure the probe-induced density modulation $\langle\delta\hat{\rho}_e\rangle$, where $\delta\hat{\rho}_e$ denotes the density fluctuation operator at momenta $(\pm\hbar k, \pm\hbar k)$. We define the corresponding quadratic density response function $\mathcal{R}_\rho$ as the spectral weight of $\langle\delta\hat{\rho}_e\rangle^2$, normalized to the pump power P and the probe pulse area $\langle n_{pr}\rangle$. The response function $\mathcal{R}_N$ of the atomic population N_e in the excited momentum state $|e\rangle$ is defined in a similar way [25].

Approaching the critical point from below, a strongly increasing density response is observed (Fig. 4). This indicates the presence of enhanced density fluctuations with λ-periodic correlations in the unperturbed system. The data is in good agreement with our model (shading), which predicts $\mathcal{R}_\rho$ to scale as $(E_1/E_s)^2$ in the normal

phase, in accordance with Feynman's relation. In the supersolid phase, the density response decreases again as a function of P, as expected for the increasing excitation energy (Fig. 3). A similar behavior is observed for the response in the momentum state population N_e (Fig. 4, inset), which exhibits a larger sensitivity to variations of the relative phase φ [25]. For positive interaction V (Fig. 4, inset), the response of the system is reduced with respect to the non-interacting case, $V = 0$.

We have observed a roton-type mode softening causing a superfluid-to-supersolid transition in a model system for long-range interactions. Increasingly complex spatial structures of long-range atom-atom interactions [28–30] can be tailored by extending the experimental setup to multiple cavity modes.

* esslinger@phys.ethz.ch

[1] I. Bloch, J. Dalibard, W. Zwerger, *Rev. Mod. Phys.* **80**, 885 (2008).

[2] A. Griesmaier, J. Werner, S. Hensler, J. Stuhler, T. Pfau, *Phys. Rev. Lett.* **94**, 160401 (2005).

[3] K.-K. Ni, *et al.*, *Science* **322**, 231 (2008).

[4] J. Deiglmayr, *et al.*, *Phys. Rev. Lett.* **101**, 133004 (2008).

[5] M. Lu, N. Q. Burdick, S. H. Youn, B. L. Lev, *Phys. Rev. Lett.* **107**, 190401 (2011).

[6] T. Lahaye, C. Menotti, L. Santos, M. Lewenstein, T. Pfau, *Rep. Prog. Phys.* **72**, 126401 (2009).

[7] L. Santos, G. V. Shlyapnikov, M. Lewenstein, *Phys. Rev. Lett.* **90**, 250403 (2003).

[8] D. H. J. O'Dell, S. Giovanazzi, G. Kurizki, *Phys. Rev. Lett.* **90**, 110402 (2003).

[9] R. W. Cherng, E. Demler, *Phys. Rev. Lett.* **103**, 185301 (2009).

[10] N. Henkel, R. Nath, T. Pohl, *Phys. Rev. Lett.* **104**, 195302 (2010).

[11] J. L. Yarnell, G. P. Arnold, P. J. Bendt, E. C. Kerr, *Phys. Rev. Lett.* **1**, 9 (1958).

[12] Y. Pomeau, S. Rica, *Phys. Rev. Lett.* **72**, 2426 (1994).

[13] T. Lahaye, *et al.*, *Nature* **448**, 672 (2007).

[14] M. Fattori, *et al.*, *Phys. Rev. Lett.* **101**, 190405 (2008).

[15] G. Bismut, *et al.*, *Phys. Rev. Lett.* **105**, 040404 (2010).

[16] T. Koch, *et al.*, *Nature Phys.* **4**, 218 (2008).

[17] P. Münstermann, T. Fischer, P. Maunz, P. W. H. Pinkse, G. Rempe, *Phys. Rev. Lett.* **84**, 4068 (2000).

[18] J. K. Asbóth, P. Domokos, H. Ritsch, *Phys. Rev. A* **70**, 013414 (2004).

[19] C. Maschler, H. Ritsch, *Phys. Rev. Lett.* **95**, 260401 (2005).

[20] S. Slama, G. Krenz, S. Bux, C. Zimmermann, P. W. Courteille, *AIP Conf. Proc.* **970**, 319 (2008).
[21] P. Domokos, H. Ritsch, *Phys. Rev. Lett.* **89**, 253003 (2002).
[22] D. Nagy, G. Szirmai, P. Domokos, *Eur. Phys. J. D* **48**, 127 (2008).
[23] K. Baumann, C. Guerlin, F. Brennecke, T. Esslinger, *Nature* **464**, 1301 (2010).
[24] J. Stenger, *et al.*, *Phys. Rev. Lett.* **82**, 4569 (1999).
[25] See supporting material on Science Online.
[26] J. Steinhauer, R. Ozeri, N. Katz, N. Davidson, *Phys. Rev. Lett.* **88**, 120407 (2002).
[27] P. Nozières, D. Pines, *The Theory of Quantum Liquids*, vol. II (Addison-Wesley, Reading, MA, 1990).
[28] S. Gopalakrishnan, B. L. Lev, P. M. Goldbart, *Nature Phys.* **5**, 845 (2009).
[29] P. Strack, S. Sachdev, *Phys. Rev. Lett.* **107**, 277202 (2011).
[30] S. Gopalakrishnan, B. L. Lev, P. M. Goldbart, *Phys. Rev. Lett.* **107**, 277201 (2011).

SUPPLEMENTARY MATERIALS

We give details of the experimental setup and provide a theoretical description of the dispersively coupled condensate-cavity system. An effective Hamiltonian for the cavity-mediated long-range interaction is derived. Based on a mean-field description, we numerically calculate the steady state of the system including contact interactions and the transverse lattice potential. We deduce in a Bogoliubov approach the energy of collective excitations, which softens towards the critical point. The time evolution of the system during probing is derived and a diverging response to density perturbations at the phase transition is found.

Experimental details

The atoms are prepared in the hyperfine state $(F, m_F) = (1, -1)$ with respect to a quantization axis pointing along the cavity axis, where F is the total angular momentum and m_F the magnetic quantum number. The transverse pump laser with wavelength $\lambda = 784.5\,\text{nm}$ is linearly polarized along the y-axis (see Fig. 1 in the main text) and off-resonantly drives, via the atoms, two degenerate cavity TEM_{00} modes with circular polarizations ϵ_+ and ϵ_-. The ratio of the corresponding two-photon Rabi frequencies is given by $\eta_+/\eta_- = 3.26/1.25$, where all allowed dipole transitions in the D_1 and D_2 lines of ^{87}Rb have been taken into account. The maximum dispersive shift of the two cavity modes induced by a single maximally coupled atom is $U_0^+ = 2\pi \times 87\,\text{Hz}$ and $U_0^- = 2\pi \times 33\,\text{Hz}$, respectively. The transverse pump laser induces an optical lattice potential along the z-axis with periodicity of $\lambda/2$. Its depth V_p is calibrated using Raman-Nath diffraction [31] and takes for our experimental parameters a value of $3E_\text{r}$ at the critical point, with recoil energy $E_\text{r} = \frac{\hbar^2 k^2}{2m}$, wavevector $k = 2\pi/\lambda$, and atomic mass m. In the theoretical analysis, the Gaussian envelopes of the pump and cavity fields along the transverse directions [32] are effectively taken into account by weighted averages of V_p, $\eta_\pm$ and $U_0^\pm$ over the spatial extent of the atomic cloud. The Thomas-Fermi radii of the condensate in the external harmonic trapping potential are given by $(R_x, R_y, R_z) = (3.5, 18.3, 3.7)\,\mu\text{m}$, assuming an atom number of $N = 1.65 \times 10^5$.

The length $(176\,\mu\text{m})$ of the cavity is actively stabilized using a laser with a wavelength of $830\,\text{nm}$, which is referenced onto the transverse pump laser. The depth of the resulting intracavity lattice potential was measured to be $0.04(2)E_\text{r}$, and is neglected in the theoretical analysis. Transverse pump light and cavity probe light propagate through independent optical fibers, resulting in a variation of their relative phase φ between different experimental runs. The cavity output light is monitored on a single-photon counting module with an overall detection

efficiency of intracavity photons of 4(1)%. For the data taken in the normal phase, the critical pump power P_{cr} was deduced from the intracavity photon number monitored during independent sweeps across the phase transition.

Theoretical description of the coupled condensate-cavity system

The coupled condensate-cavity system is described in a many-body formalism following Ref. [33, 34]. By adiabatically eliminating the fast cavity field dynamics, we derive an effective Hamiltonian, which describes the long-range atom-atom interaction.

After adiabatically eliminating the electronically excited states, the transversally driven condensate-cavity system is described by the many-body Hamiltonian $\hat{H} = \hat{H}_{\mathrm{c}} + \hat{H}_{\mathrm{a}} + \hat{H}_{\mathrm{a-c}}$, where

$$
\begin{aligned}
\hat{H}_{\mathrm{c}} &= -\hbar\Delta_{\mathrm{c}}\hat{a}^\dagger\hat{a} \\
\hat{H}_{\mathrm{a}} &= \int d^3 r \hat{\Psi}^\dagger(\mathbf{r})\left[\frac{\mathbf{p}^2}{2m} + V_{\mathrm{p}}\cos^2(kz)\right. \\
&\quad \left. + \frac{g}{2}\hat{\Psi}^\dagger(\mathbf{r})\hat{\Psi}(\mathbf{r})\right]\hat{\Psi}(\mathbf{r}) \\
\hat{H}_{\mathrm{a-c}} &= \int d^3 r \hat{\Psi}^\dagger(\mathbf{r})\left[\hbar\eta\cos(kx)\cos(kz)(\hat{a}+\hat{a}^\dagger)\right. \\
&\quad \left. + \hbar U_0\cos^2(kx)\hat{a}^\dagger\hat{a}\right]\hat{\Psi}(\mathbf{r}),
\end{aligned}
$$
(S1)

with bosonic atomic field operator $\hat{\Psi}(\mathbf{r})$ and photon operators $\hat{a}$ and $\hat{a}^\dagger$. To keep the notation simple we describe only one of the two circularly polarized TEM_{00} cavity modes. Final results will be given for the case of two cavity modes.

In equation (S1), $\hat{H}_{\mathrm{c}}$ describes the dynamics of a single TEM_{00} cavity mode with spatial mode function $\cos(kx)$, whose frequency ω_{c} is detuned by $\Delta_{\mathrm{c}} = \omega_{\mathrm{p}} - \omega_{\mathrm{c}}$ from the pump laser frequency ω_{p}. The term $\hat{H}_{\mathrm{a}}$ captures the atomic evolution in the transverse optical lattice potential with depth V_{p}, including contact interactions with strength $g = \frac{4\pi\hbar^2 a}{m}$, where a denotes the s-wave scattering length. The interaction between the atoms and the pump and cavity light fields is governed by $\hat{H}_{\mathrm{a-c}}$. The first term describes light scattering between pump and cavity field at a rate which is determined by the maximum two-photon Rabi frequency η. The second term accounts for the dispersive shift of the cavity resonance frequency with light-shift U_0 of a single maximally coupled atom.

As the cavity field reaches a steady-state on a time scale fast compared to atomic motion, its equation of motion can be formally solved, yielding

$$
\hat{a} = \frac{\eta\hat{\Theta}}{(\Delta_{\mathrm{c}} - U_0\hat{\mathcal{B}}) + i\kappa}
$$
(S2)

with the cavity field decay rate $\kappa = 2\pi \times 1.25$ MHz. Due to Bragg scattering of pump light, the intracavity field amplitude is proportional to the order parameter $\hat{\Theta} = \int d^3 r \, \hat{\Psi}^\dagger(\mathbf{r})\cos(kx)\cos(kz)\hat{\Psi}(\mathbf{r})$ which measures the atomic density modulation on the checkerboard pattern $\cos(kx)\cos(kz)$. The overall dispersive shift of the empty cavity resonance caused by the presence of the atoms is proportional to the bunching parameter $\hat{\mathcal{B}} = \int d^3 r \, \hat{\Psi}^\dagger(\mathbf{r})\cos^2(kx)\hat{\Psi}(\mathbf{r})$.

After eliminating the steady-state cavity field of Eq. (S2) from Hamiltonian Eq. (S1), an effective Hamiltonian description is obtained (see main text, Eq. 1):

$$
\begin{aligned}
\hat{H}_{\mathrm{eff}} = \; &\hat{H}_{\mathrm{a}} + V\int d^3\mathbf{r}d^3\mathbf{r}'\hat{\Psi}^\dagger(\mathbf{r})\hat{\Psi}^\dagger(\mathbf{r}')\cos(kx)\cos(kz) \\
&\times \cos(kx')\cos(kz')\hat{\Psi}(\mathbf{r})\hat{\Psi}(\mathbf{r}').
\end{aligned}
$$
(S3)

The strength V of this cavity-mediated atom-atom interaction is given by $V = \hbar\frac{\eta^2\tilde{\Delta}_{\mathrm{c}}}{\tilde{\Delta}_{\mathrm{c}}^2+\kappa^2} \approx \hbar\frac{\eta^2}{\tilde{\Delta}_{\mathrm{c}}}$, where the detuning of the pump laser from the dispersively shifted cavity resonance $\tilde{\Delta}_{\mathrm{c}} = \Delta_{\mathrm{c}} - U_0\mathcal{B}_0$ was taken to be large compared to the cavity half-linewidth κ. Here, $\mathcal{B}_0 = \langle\hat{\mathcal{B}}\rangle$ denotes the bunching parameter in the steady state. In a quantized picture, $NV/\hbar$ corresponds to the rate at which cavity photons are exchanged between atoms, as shown exemplarily in the zoom of Fig. 1A in the main text.

The effective Hamiltonian Eq. (S3) describes a closed system and neglects dynamical and quantum backaction effects originating from cavity decay and cavity input noise. This is justified on short timescales as long as $|\tilde{\Delta}_{\mathrm{c}}| \gg \kappa \gg E_{\mathrm{r}}/\hbar$ [35].

Mean-field description in the steady state

Based on a mean-field description [36], we derive a numerical solution of the steady state of the system.

A mean-field description of the system is obtained by formally replacing the operators $\hat{\Psi}$ and $\hat{a}$ in Eq. (S1) with the atomic mean-field $\sqrt{N}\psi_0$ and the coherent cavity amplitude α_0, respectively. Their steady-state values are determined by the non-local Gross-Pitaevskii equation

$$
\begin{aligned}
\mu_0\psi_0(x,z) = \Big(&\frac{-\hbar^2}{2m}(\partial_x^2 + \partial_z^2) + V_{\mathrm{p}}(z) + \hbar U_0(x)|\alpha_0|^2 \\
&+ \hbar\eta(x,z)(\alpha_0 + \alpha_0^*) + g_{\mathrm{2D}}|\psi_0|^2\Big)\psi_0(x,z)
\end{aligned}
$$
(S4)

with $\alpha_0 = \frac{\eta\Theta_0}{\tilde{\Delta}_{\mathrm{c}}+i\kappa}$ and the chemical potential μ_0. Here, we introduced the steady state order parameter $\Theta_0 = N\langle\psi_0|\cos(kx)\cos(kz)|\psi_0\rangle$ and bunching parameter $\mathcal{B}_0 = N\langle\psi_0|\cos^2(kx)|\psi_0\rangle$, as well as the notations $V_{\mathrm{p}}(z) = V_{\mathrm{p}}\cos^2(kz)$, $\eta(x,z) = \eta\cos(kx)\cos(kz)$ and $U_0(x) =$

$U_0 \cos^2(kx)$. We reduced the description in Eq. (S4) to the pump and cavity directions, assuming a homogeneous condensate density along the weakly confined y-axis. The contact interaction strength is accordingly replaced by $g_{2D} = \lambda^2 \bar{n} g$ with average 3D condensate density $\bar{n}$ and the normalization condition $\int_0^\lambda dx \int_0^\lambda dz \, |\psi_0|^2 = 1$ [37].

For negative $\tilde{\Delta}_c$, Eq. (S4) exhibits a dynamical instability above a critical transverse pump power P_{cr}, driving the system from a normal phase into a supersolid phase with λ-periodic density modulation. In the normal phase, $P < P_{cr}$, the condensate density is flat along the cavity axis, resulting in a vanishing order parameter, $\Theta_0 = 0$, and cavity field amplitude, $\alpha_0 = 0$. The mean-field solution ψ_0 is given by the lowest energy Bloch state in the shallow optical lattice potential of the transverse pump field. In the supersolid phase, $P > P_{cr}$, the atomic cloud exhibits a λ-periodic density modulation both along the transverse and the cavity direction. Correspondingly, the order parameter takes a finite value, $\Theta_0 \neq 0$, and light scattering off the diagonal Bragg planes results in a coherent cavity field amplitude, $\alpha_0 \neq 0$. The mean-field solution ψ_0 is given by the minimal energy state in the two-dimensional lattice potential originating from interference between the transverse and cavity field. In the supersolid phase, the emergent checkerboard density modulation locks to one of two possible sublattices, which are spatially shifted by $\lambda/2$ and have opposite signs of Θ_0 and α_0. As both solutions share the same excitation spectrum, we assume $\Theta_0 > 0$ in the following.

We numerically find the ground state ψ_0 of the system by propagating Eq. (S4) in imaginary time, using a computational cell of size λ^2 with periodic boundary conditions. We include the recorded steady state mean intracavity photon number $|\alpha_0|^2$ and the experimentally calibrated lattice depth V_p in the calculations.

Deriving the collective excitation spectrum

We describe collective excitations on top of the mean-field solution. To this end, we calculate the Bogoliubov excitations in the steady-state lattice potential and identify a single excitation mode which is dominantly affected by the long-range interactions. We diagonalize the resulting truncated Hamiltonian and deduce the energy of collective excitations.

Following Ref. [36], we expand the atomic and cavity field operators around their mean-field solution (ψ_0, α_0) according to

$$\hat{\Psi} = (\sqrt{N}\psi_0 + \delta\hat{\Psi})e^{-it\mu_0/\hbar}$$
$$\hat{a} = \alpha_0 + \delta\hat{a}. \tag{S5}$$

Here, the linearized cavity field fluctuation operator

$$\delta\hat{a} = \frac{\eta}{\tilde{\Delta}_c + i\kappa}\left[\delta\hat{\Theta} + \frac{\Theta_0 U_0}{\tilde{\Delta}_c + i\kappa}\delta\hat{\mathcal{B}}\right]. \tag{S6}$$

is given in terms of the operators $\delta\hat{\Theta} = \sqrt{N}\int d^3r\,(\delta\hat{\Psi}^\dagger + \delta\hat{\Psi})\cos(kx)\cos(kz)\psi_0$ and $\delta\hat{\mathcal{B}} = \sqrt{N}\int d^3r\,(\delta\hat{\Psi}^\dagger + \delta\hat{\Psi})\cos^2(kx)\psi_0$, describing fluctuations of the order and bunching parameter around their steady-state values Θ_0 and $\mathcal{B}_0$, taking ψ_0 to be real-valued.

After eliminating the cavity field fluctuation $\delta\hat{a}$, assuming $\tilde{\Delta}_c^2 \gg \kappa^2$, and keeping only linear terms in the equation of motion for $\delta\hat{\Psi}$, we arrive at a quadratic Hamiltonian

$$\hat{H}_{exc} = \hat{H}_0 + V\left[\delta\hat{\Theta} + \frac{\Theta_0 U_0}{\tilde{\Delta}_c}\delta\hat{\mathcal{B}}\right]^2 \tag{S7}$$

describing the dynamics of atomic fluctuations around the mean-field solution. The first term $\hat{H}_0$ captures the dynamics in the static steady-state lattice potential including contact interactions, and is given by

$$\hat{H}_0 = \int d^3r \, \delta\hat{\Psi}^\dagger\left[\frac{-\hbar^2}{2m}(\partial_x^2 + \partial_z^2) + V_p(z)\right.$$
$$\left. + \hbar\eta(x,z)(\alpha_0 + \alpha_0^*) + \hbar U_0(x)|\alpha_0|^2\right]\delta\hat{\Psi}$$
$$+ \frac{1}{2}\,g_{2D}\,\psi_0^2\left(\delta\hat{\Psi}^2 + (\delta\hat{\Psi}^\dagger)^2\right) + 2g_{2D}|\psi_0|^2\delta\hat{\Psi}^\dagger\delta\hat{\Psi}. \tag{S8}$$

The second term in Eq. (S7) describes how atomic density fluctuations are affected by the cavity-mediated long-range interaction.

In the normal phase, $\hat{H}_{exc}$ is directly obtained from Eq. (S3) by quadratic expansion in $\delta\hat{\Psi}$ around the steady state. In the supersolid phase, the dispersive cavity shift, which depends on the atomic density distribution, gives rise to an additional long-range interaction term with $\lambda/2$-periodicity along the cavity axis [34], whose strength is proportional to the order parameter Θ_0. However, as the order parameter vanishes at the critical point, solely the term $\delta\hat{\Theta}^2$ in Eq. (S7) induces the normal to supersolid phase transition.

To find the energy of collective excitations described by $\hat{H}_{exc}$, we first calculate the elementary excitations of $\hat{H}_0$ using the Bogoliubov ansatz [38, 39]

$$\delta\hat{\Psi}(\mathbf{r}) = \sum_j \left(u_j(\mathbf{r})\hat{c}_j + v_j^*(\mathbf{r})\hat{c}_j^\dagger\right), \tag{S9}$$

with band index j, Bogoliubov modes $u_j(\mathbf{r})$ and $v_j(\mathbf{r})$, and corresponding mode operators $\hat{c}_j$, fulfilling bosonic commutation relations. In this basis the Hamiltonian $\hat{H}_{exc}$ reads

$$\hat{H}_{exc} = \sum_j \left(E_j\hat{c}_j^\dagger\hat{c}_j + NV\chi_j(\hat{c}_j + \hat{c}_j^\dagger)^2\right), \tag{S10}$$

with Bogoliubov energies E_j and interaction matrix elements

$$\chi_j = \left\langle\psi_0\left|\cos(kx)\cos(kz) + \frac{\Theta_0 U_0}{\tilde{\Delta}_c}\cos^2(kx)\right|u_j + v_j\right\rangle^2. \tag{S11}$$

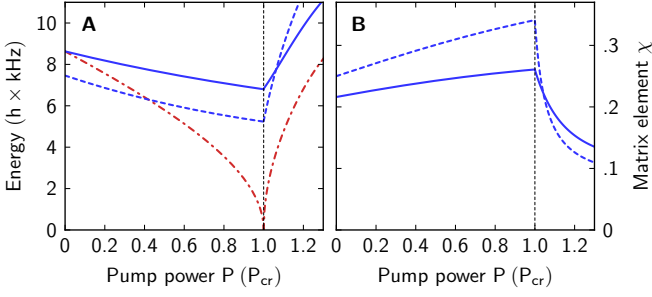FIG. 5. (**A**) Bare energies (blue) of the excited state with maximum matrix element χ in the normal and supersolid phase. Dashed and solid blue lines correspond to the case of vanishing and present contact atom-atom interactions. The red dashed-dotted line shows the soft mode energy in the presence of long-range and contact atom-atom interactions. (**B**) Maximum matrix element χ in the presence (solid) and absence (dashed) of contact atom-atom interactions.

From a numerical calculation of the matrix elements χ_j we find in our parameter regime only a single Bogoliubov mode exhibiting a relevant matrix element χ_j for energies up to $15E_{\rm r}$. All other matrix elements χ_j are suppressed by more than two orders of magnitude. In the normal phase the maximally coupled excited mode lies in the lowest energy band of the transverse lattice potential with quasi-momentum $(q_x, q_z) = (\pm\hbar k, \pm\hbar k)$. In the supersolid phase this state is folded into the third band at the center of the Brillouin zone as a result of the emerging λ-periodicity.

In terms of the excited mode with dominant matrix element χ_j, which we denote in the following by the index $j = 1$, the effective Hamiltonian reduces to

$$\hat{H}_{\rm exc} = E_1 \hat{c}_1^\dagger \hat{c}_1 + NV\chi(\hat{c}_1 + \hat{c}_1^\dagger)^2 \quad \text{(S12)}$$

with $\chi = \chi_1$. In the absence of the transverse lattice potential and contact atom-atom interactions, $\hat{H}_{\rm exc}$ reduces in the normal phase to the Hamiltonian given in the main text, Eq. 2.

We obtain the soft mode energy spectrum by diagonalizing Hamiltonian $\hat{H}_{\rm exc}$ in terms of a second Bogoliubov transformation $\hat{b} = \mu\hat{c}_1 + \nu\hat{c}_1^\dagger$. Up to a constant term, this yields $\hat{H}_{\rm exc} = E_{\rm s}\hat{b}^\dagger\hat{b}$ with soft mode energy

$$E_{\rm s} = E_1\sqrt{1 + \frac{4NV\chi}{E_1}}. \quad \text{(S13)}$$

For $V < 0$, $E_{\rm s}$ softens towards the phase transition and vanishes at $V_{\rm cr} = -E_1^{\rm cr}/(4N\chi_{\rm cr})$ with $(E_1^{\rm cr}, \chi_{\rm cr}) = (E_1, \chi)|_{P=P_{\rm cr}}$. In the supersolid phase, the excitation energy rises again due to competition between the increasing Bogoliubov energy E_1 and the decreasing interaction energy which is proportional to the matrix element χ (see Fig. S5).

Results for two circularly polarized cavity modes $\hat{a}_\pm$ are obtained by replacing $V\chi$ in (S12) and (S13) by $\sum_{n=\pm} V_n\chi_n$, with $V_\pm$ and $\chi_\pm$ deduced accordingly from the cavity parameters $(\eta_\pm, U_0^\pm)$. The calculated energy spectrum shown in Fig. 3 takes into account the experimentally calibrated depth of the transverse lattice potential and the measured steady-state intracavity photon number $|\alpha_0|^2$ in the presence of atoms. Systematic uncertainties of these quantities are estimated to be 10% and 25%, respectively (see shaded regions in Fig. 3).

Probing the collective excitation spectrum

By integrating the equation of motion of the atomic field, we predict the build-up of atomic excitations and of the cavity light field during probing.

To probe the excitation spectrum, we weakly drive the cavity field with amplitude $\eta_{\rm pr}(t)$ and frequency $\omega_{\rm pr}$. This is described by the driving Hamiltonian $-\hbar\eta_{\rm pr}(t)(\hat{a}e^{i(\delta t+\varphi)} + \hat{a}^\dagger e^{-i(\delta t+\varphi)})$ with probe-pump detuning $\delta = \omega_{\rm pr} - \omega_{\rm p}$ and relative phase φ between probe and pump beam. The resulting coherent intracavity probe field is given by

$$\alpha_{\rm pr}(t) = -\frac{\eta_{\rm pr}(t)e^{-i(\delta t+\varphi)}}{\tilde{\Delta}_{\rm c} + i\kappa}. \quad \text{(S14)}$$

Interference of the probe field with the transverse pump field and the steady-state cavity field α_0 results in a modulated lattice potential. The corresponding perturbation of the atomic field is given by

$$\hat{H}_{\rm pr} = \hbar\xi(t)\left[\delta\hat{\Theta} + \frac{U_0\Theta_0}{\tilde{\Delta}_{\rm c} + i\kappa}\delta\hat{\mathcal{B}}\right]\cos(\delta t + \varphi), \quad \text{(S15)}$$

with perturbation amplitude $\xi(t) = 2\eta\sqrt{n_{\rm pr}(t)}$ and mean intracavity photon number $n_{\rm pr}(t) = \frac{\eta_{\rm pr}^2(t)}{\tilde{\Delta}_{\rm c}^2 + \kappa^2}$. As $|\tilde{\Delta}_{\rm c}| \gg \kappa$ in the experiment, we set the phase shift, originating from coupling into the cavity, to π. In terms of the mode operator $\hat{c}_1$, the perturbation reads

$$\hat{H}_{\rm pr} = \hbar\xi(t)\sqrt{N\chi}(\hat{c}_1 + \hat{c}_1^\dagger)\cos(\delta t + \varphi). \quad \text{(S16)}$$

To quantify the response on this perturbation, we evolve the Hamiltonian $\hat{H} = \hat{H}_{\rm exc} + \hat{H}_{\rm pr}$ in time according to the Heisenberg equation

$$\begin{aligned} i\hbar\dot{\hat{c}}_1 = &E_1\hat{c}_1 + 2NV\chi(\hat{c}_1 + \hat{c}_1^\dagger) \\ &+ \hbar\xi(t)\sqrt{N\chi}\cos(\delta t + \varphi) - i\hbar\gamma\hat{c}_1. \end{aligned} \quad \text{(S17)}$$

Motivated by our experimental observations, we phenomenologically introduced a damping term with damping constant γ into the time evolution of $\hat{c}_1$. This accounts for possible damping mechanisms like s-wave scattering with other momentum modes, trap loss or finite-size dephasing. The general solution of Eq. (S17) reads

$$\hat{c}_1(t) = 2\eta\sqrt{N\chi n_{\rm pr,0}}\left(\frac{E_1}{E_{\rm s}}\text{Im}(\mathcal{Y}(t)) + i\text{Re}(\mathcal{Y}(t))\right). \quad \text{(S18)}$$

Here,

$$\mathcal{Y}(t) = e^{(i\omega_s - \gamma)t} \int_0^t dt'\, e^{-(i\omega_s - \gamma)t'} \cos(\delta t' + \varphi)\Pi(t')\,,$$
(S19)

with $\omega_s = E_s/\hbar$ and $n_{pr}(t) = n_{pr,0}\Pi(t)^2$. Here, the envelope function $\Pi(t)$ of the probe pulse with duration τ and the maximum probe photon number $n_{pr,0}$ were introduced. The population of the excited momentum mode and the mean intracavity photon number are directly obtained from Eq. (S18)

$$N_1(t) = \langle \hat{c}_1^\dagger \hat{c}_1 \rangle$$
$$= 4\eta^2 n_{pr,0}\, N\, \chi \left[\left(\frac{E_1}{E_s}\right)^2 \text{Im}(\mathcal{Y}(t))^2 + \text{Re}(\mathcal{Y}(t))^2 \right]$$

$$n_{ph}(t) = \left| \alpha_0 - \frac{4\eta^2\sqrt{n_{pr,0}}N\chi}{\tilde{\Delta}_c + i\kappa}\left(\frac{E_1}{E_s}\right)\text{Im}(\mathcal{Y}(t)) \right.$$
$$\left. + \sqrt{n_{pr}(t)}e^{-i(\delta t + \varphi)} \right|^2.$$
(S20)

The second term in $n_{ph}(t)$ describes the pump field which was Bragg scattered off the excited density modulation into the cavity mode. From N_1, the population N_e in the momentum state $|e\rangle$ is obtained according to $N_e = \zeta N_1$, where ζ denotes the absolute square of the Fourier amplitude of the excited Bogoliubov mode $u_1 + v_1$ at momenta $(\pm\hbar k, \pm\hbar k)$.

The curves shown in Fig. 2C and D of the main text are obtained from Eqs. (3), where the phase φ was adjusted to fit the data in Fig. 2C. The resonance curves, displayed in Fig. 2B and E of the main text, correspond to phase-averaged values $\langle N_e(\tau)\rangle_{\varphi\in[0,2\pi]}$ and $\langle\int_0^\tau dt\, n_{ph}(t)/\tau\rangle_{\varphi\in[0,2\pi]}$ where the resonance frequency ω_s and the amplitude $\eta^2 N\chi$ were adjusted independently to fit the data. Due to the detection background an offset was added to $N_e(\tau)$. The standard deviation of fluctuations associated with the uncontrolled relative phase φ is displayed by the shadings in Fig. 2B and E of the main text.

Response in atomic density and momentum state population

Bragg spectroscopy, as described by the density perturbation $\hat{H}_{pr}$, induces a response in the atomic density and in the population of the excited state. Normalized to the integrated amplitude of the perturbation, this density response is a measure for the susceptibility of the system on an external density perturbation and provides at zero temperature a direct link to the static structure factor [38, 40]. We use the recorded modulation $\langle\delta\hat{a}\rangle$ of the intracavity field to quantify the density response $\langle\delta\hat{\rho}\rangle$ of the system.

Consider the density operator $\hat{\rho}(\mathbf{r}) = \hat{\Psi}^\dagger(\mathbf{r})\hat{\Psi}(\mathbf{r})$ and its linear expansion $\hat{\rho} = \rho_0 + \delta\hat{\rho} = N|\psi_0|^2 + \sqrt{N}\psi_0(\delta\hat{\Psi}^\dagger +$ $\delta\hat{\Psi}$) around the equilibrium value $\rho_0 = \langle\hat{\rho}\rangle$. In terms of the density fluctuation operator in Fourier space, defined as $\delta\hat{\rho}_\mathbf{k} = \int d^3r\, e^{-i\mathbf{kr}}\delta\hat{\rho}(\mathbf{r})$, the fluctuations of the order and bunching parameter $\delta\hat{\Theta}$ and $\delta\hat{\mathcal{B}}$ read

$$\delta\hat{\Theta} = \sum_{\mathbf{k}\in(\pm k,\pm k)} \delta\hat{\rho}_\mathbf{k}/4 \quad \text{and} \quad \delta\hat{\mathcal{B}} = \sum_{\mathbf{k}\in(\pm 2k,0)} \delta\hat{\rho}_\mathbf{k}/4\,.$$

Fluctuations of the cavity field $\delta\hat{a}$, see Eq. (S6), are thus given by

$$\delta\hat{a} = \frac{\eta}{4(\tilde{\Delta}_c + i\kappa)}\left[\sum_{\mathbf{k}\in(\pm k,\pm k)} \delta\hat{\rho}_\mathbf{k} + \frac{\Theta_0 U_0}{\tilde{\Delta}_c + i\kappa}\sum_{\mathbf{k}\in(\pm 2k,0)}\delta\hat{\rho}_\mathbf{k} \right]\,,$$

and provide a measure of the induced atomic density modulation. We define the corresponding (quadratic) density response function

$$\mathcal{R}_\rho = \frac{1}{P\int_0^\tau n_{pr}(t)dt}\int_{-\infty}^\infty d\delta \left\langle \int_0^\tau \frac{|\langle\delta\hat{a}\rangle|^2 dt}{|\eta/(4(\tilde{\Delta}_c + i\kappa))|^2} \right\rangle_{\varphi\in[0,2\pi]},$$

where again an average over the relative phase φ is performed.

Experimentally, we extract $|\langle\delta\hat{a}\rangle|^2$ from the resonance fits based on Eq. (3) (see Fig. 2E in the main text), with experimentally calibrated $|\alpha_0|^2$ and n_{pr}. In order to probe the linear response of the system, the probe power was accordingly lowered when approaching the critical point. The lowest perturbation applied in the normal phase corresponds to 30(8) intracavity probe photons in total.

Similarly, the response function $\mathcal{R}_N$ associated with the detected number of atoms with momenta $(\pm\hbar k, \pm\hbar k)$ is defined as

$$\mathcal{R}_N = \frac{1}{P\int_0^\tau dt\, n_{pr}(t)}\int_{-\infty}^\infty d\delta\,\langle N_e(\tau)\rangle_{\varphi\in[0,2\pi]}.$$

which is proportional to the area below the fitted resonances of $N_e(\tau)$, see Fig. 2B in the main text.

The dominant scaling factor of $\mathcal{R}_\rho$ when approaching the critical point is found from Eq. (3) to be $(E_1/E_s)^2$. As $\mathcal{R}_\rho$ measures the quadratic density response, this is in agreement with Feynman's relation, given in the main text. Since $N_e(\tau)$ is sensitive to both quadratures of $\hat{c}_1$ (see Eq. (3)), the response function $\mathcal{R}_N$ scales differently and exhibits larger variances in the relative phase φ.

---

* esslinger@phys.ethz.ch

[31] O. Morsch, M. Oberthaler, *Rev. Mod. Phys.* **78**, 179 (2006).

[32] K. Baumann, C. Guerlin, F. Brennecke, T. Esslinger, *Nature* **464**, 1301 (2010).

[33] C. Maschler, H. Ritsch, *Phys. Rev. Lett.* **95**, 260401 (2005).

[34] C. Maschler, I. B. Mekhov, H. Ritsch, *Eur. Phys. J. D* **46**, 545 (2008).

[35] D. Nagy, G. Konya, G. Szirmai, P. Domokos, *Phys. Rev. Lett.* **104**, 130401 (2010).

[36] D. Nagy, G. Szirmai, P. Domokos, *Eur. Phys. J. D* **48**, 127 (2008).

[37] M. Krämer, C. Menotti, L. Pitaevskii, S. Stringari, *The European Physical Journal D - Atomic, Molecular, Opti-*

cal and Plasma Physics **27**, 247 (2003).

[38] L. Pitaevskii, S. Stringari, *Bose-Einstein Condensation* (Oxford University Press, 2003).

[39] Y. Castin, *Coherent atomic matter waves* (Springer Berlin, 2001), vol. 72, chap. Course 1: Bose-Einstein Condensates in Atomic Gases: Simple Theoretical Results, pp. 1–136.

[40] R. Ozeri, N. Katz, J. Steinhauer, N. Davidson, *Rev. Mod. Phys.* **77**, 187 (2005).